

Collapsing domain walls with \mathbb{Z}_2 -violating coupling to thermalized fermions and their impact on gravitational wave detections

Qing-Quan Zeng,¹ Xi He,¹ Zhao-Huan Yu,^{1,*} and Jiaming Zheng[†]

¹*School of Physics, Sun Yat-Sen University, Guangzhou 510275, China*

We study the dynamics of domain walls formed through the spontaneous breaking of an approximate \mathbb{Z}_2 symmetry in a scalar field, focusing on their collapse under the influence of quantum and thermal corrections induced by a \mathbb{Z}_2 -violating Yukawa coupling to Dirac fermions in the thermal bath. The thermal effects render the potential bias between the true and false vacua temperature-dependent and may lead to notable variations in the annihilation temperature of domain walls, in addition to the shift caused by temperature-independent quantum corrections. These modifications could substantially alter the gravitational wave spectrum produced by collapsing domain walls, potentially providing observable signatures for future gravitational wave detection experiments.

CONTENTS

I. Introduction	2
II. A Toy Model of Asymmetric Yukawa Coupling and Its Thermal Corrections	3
III. Evolution of domain walls	5
IV. Spectrum of gravitational waves	13
V. Summary	15
Acknowledgments	17
References	17

* Corresponding author. yuzhaoh5@mail.sysu.edu.cn

† Corresponding author. zhengjm3@gmail.com

I. INTRODUCTION

Since the ground-breaking observations of gravitational wave (GW) events by the LIGO-Virgo Collaboration [1, 2], the possibility of detecting gravitational wave signals in the early universe has drawn tremendous attention in physics research. Various well-motivated hypothesized processes in the primordial universe, such as cosmic inflation, cosmological phase transitions, and the evolution of topological defects, naturally source stochastic gravitational wave background (SGWB) that may be accessible by future GW experiments [3, 4], e.g., ground-based interferometers in the frequency band $10\text{--}10^3$ Hz [5, 6], pulsar timing arrays (PTAs) in $10^{-9}\text{--}10^{-7}$ Hz [7–11], and future space-borne interferometers in $10^{-4}\text{--}10^{-1}$ Hz [12–14]. Intriguingly, several PTA collaborations have reported positive evidence recently for a nHz SGWB [15–18] that may be interpreted as the smoking gun of new physics beyond the standard model [19, 20].

In various extensions of the standard model (SM), such as the grand unification theories, the high energy theory has a large symmetry group that must be broken by heavy Higgs fields in the early universe. Depending on the symmetry-breaking pattern, the corresponding phase transition may produce topological defects such as domain walls (DWs), cosmic strings, and monopoles through the Kibble mechanism [21]. In this work, we shall focus on the evolution of domain walls, the two-dimensional topological defects formed in the scalar field that spontaneously breaks a discrete symmetry [21–24].

Stable DWs are cosmologically problematic because their energy density falls slower than those of matter and radiation and would soon overclose the universe [25, 26]. However, global symmetries are generally not expected to be exact since they are violated explicitly at least by quantum gravity effects [27, 28]. If a global discrete symmetry is only weakly broken, DWs are still produced during the phase transition. The symmetry-violating effect, usually represented by a bias term in the scalar potential [29–33], renders the DWs unstable [29, 31, 34] by sourcing pressure that tends to reduce the domains of the false vacuum. The collapsing DWs may generate a significant amount of GWs that further accelerates this process [22], and forms an SGWB that may be probed by GW experiments [29, 35–39].

In passing, we note that there exist alternative solutions to the cosmological DW problem. For instance, the DWs may be destroyed by primordial black holes [40], by cosmic string loops nucleated on the wall [41], or by cosmic strings that bound them [42], depending on the sequence symmetry-breaking. However, this work is specifically concerned with DW collapse driven by discrete symmetry-violating terms.

The evolution of the DWs with a biased scalar potential has been studied thoroughly in the literature (see, e.g., Refs. [37, 38] for reviews). However, the symmetry-breaking effect that generates the bias term in the scalar potential can also manifest in other interactions. For instance, the coupling between the scalar field and matter particles may also violate the discrete symmetry that stabilizes the DWs. If the coupled particles are rare in the universe, they only contribute to the DWs through radiative corrections [39] captured by the Coleman-Weinberg effective potential [43] at the one-loop level. On the other hand, if the particles are thermally

populated, the asymmetric interaction between the scalar field and the particles sources energy gaps between different vacua that may cause the collapse of DWs. In this work, we estimate these effects with both the Coleman-Weinberg effective potential and the thermal effective potential and determine their relative importance compared to a bias term introduced in the bare scalar potential. Then, we compute the modified GW spectrum generated by the collapse of unstable DWs and investigate its detection perspective.

The organization of this work is as follows. In Section II, we introduce the baseline model of this work that contains a real scalar field coupled to a Dirac fermionic field. Then we provide the corrections to the Lagrangian given by the Coleman-Weinberg effective potential [43, 44] and the finite temperature effective potential [45]. In Section III, we solve the configuration equation of a DW and calculate its tension. Then, we analyze the evolution of the DW network driven by the bias term to obtain its annihilation temperature. The friction exerted by the fermions in the thermal bath on the DWs is also considered. In Section IV, we demonstrate the GW spectra induced by the evolution of DWs with various benchmark parameters with and without the fermionic field, and compare them to sensitivity curves of several GW detection experiments [5–14]. Section V is the summary.

II. A TOY MODEL OF ASYMMETRIC YUKAWA COUPLING AND ITS THERMAL CORRECTIONS

We base our study on a toy model with a real scalar field ϕ that develops a domain wall configuration in the universe, and a Dirac fermionic field f that couples to the scalar. The Lagrangian is

$$\mathcal{L} = \frac{1}{2}\partial_\mu\phi\partial^\mu\phi + i\bar{f}\gamma^\mu\partial_\mu f - M_f(\phi)\bar{f}f - V_0(\phi), \quad (1)$$

where we have defined

$$M_f(\phi) \equiv m_f + y\phi, \quad (2)$$

with a mass parameter m_f and a Yukawa coupling y . The scalar potential is taken as

$$V_0(\phi) = -\frac{1}{2}\mu_\phi^2\phi^2 + \frac{1}{3}\mu_3\phi^3 + \frac{1}{4}\lambda_\phi\phi^4, \quad (3)$$

with $\mu_\phi^2 > 0$ and $\lambda_\phi > 0$. The couplings y and μ_3 violate the \mathbb{Z}_2 symmetry of the Lagrangian, $\phi \rightarrow -\phi$, explicitly. When y and μ_3 are small, the approximate \mathbb{Z}_2 symmetry of the theory is spontaneously broken by the vacuum expectation value (VEV) of ϕ and the corresponding second-order phase transition generates DWs through the Kibble mechanism [21].

At the one-loop level, the radiative correction on the scalar potential is captured by the

Coleman-Weinberg effective potentials $V_{\text{CW}}(\phi)$ [43, 44] in the $\overline{\text{MS}}$ renormalization scheme,

$$V_{\text{CW}}(\phi) = \frac{m_\phi^4(\phi)}{64\pi^2} \text{Re} \left[\ln \frac{m_\phi^2(\phi)}{\mu_{\text{R}}^2} - \frac{3}{2} \right] - \frac{M_f^4(\phi)}{16\pi^2} \left[\ln \frac{M_f^2(\phi)}{\mu_{\text{R}}^2} - \frac{3}{2} \right], \quad (4)$$

where the field-dependent scalar mass-squared is

$$m_\phi^2(\phi) \equiv \frac{\partial^2 V_0(\phi)}{\partial \phi^2}. \quad (5)$$

We fix the renormalization scale at $\mu_{\text{R}} = v_\phi$, where the VEV v_ϕ is evaluated by

$$\left. \frac{\partial}{\partial \phi} [V_0(\phi) + V_{\text{CW}}(\phi)] \right|_{\phi=v_\phi} = 0. \quad (6)$$

We assume that the f fermions and the ϕ scalar bosons are thermally produced in the early universe, which is the case if they interact efficiently with SM particles, and the finite-temperature corrections [45] to the effective scalar potential are given by

$$V_{\text{T}}(\phi, T) = \frac{T^4}{2\pi^2} \text{Re} \int_0^{+\infty} x^2 \ln \left[1 - e^{-\sqrt{x^2 + m_\phi^2(\phi)/T^2}} \right] dx \\ - \frac{2T^4}{\pi^2} \int_0^{+\infty} x^2 \ln \left[1 + e^{-\sqrt{x^2 + M_f^2(\phi)/T^2}} \right] dx. \quad (7)$$

The \mathbb{Z}_2 -violating Yukawa coupling y enters both the Coleman-Weinberg potential (4) and the thermal effective potential (7) through the field-dependent mass $M_f(\phi)$ as an additional source for the potential bias. Thus, the fully corrected effective potential is

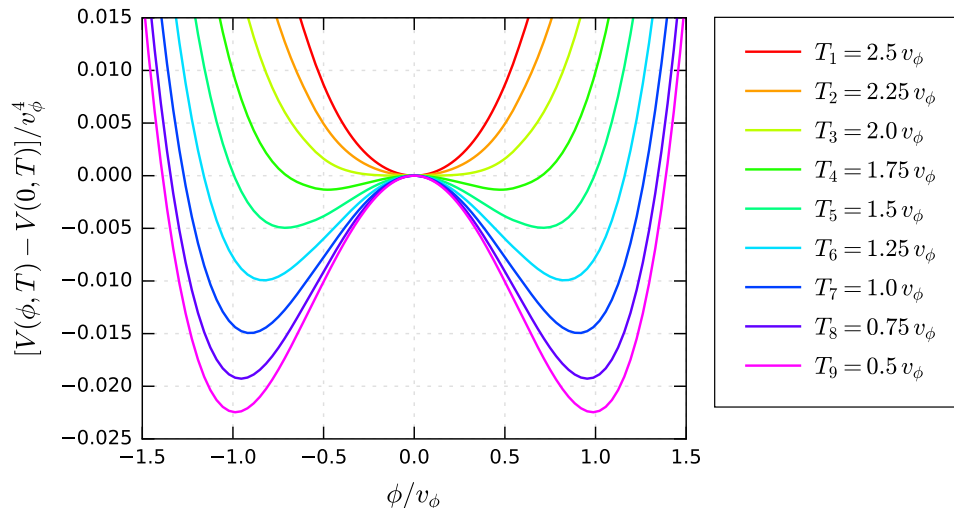
$$V(\phi, T) = V_0(\phi) + V_{\text{CW}}(\phi) + V_{\text{T}}(\phi, T). \quad (8)$$

In this work, we choose the following five parameters, μ_3 , λ_ϕ , y , m_f , and v_ϕ , as free parameters. We restrict ourselves to small \mathbb{Z}_2 -violating couplings, $\mu_3 \ll v_\phi$ and $y \ll 1$, so that they only control the late time evolution of DWs while having little impact on the phase transition and the DW formation. To illustrate our numerical results, we choose three benchmark points (BPs) of model parameters with nonzero m_f and y , and denote them as ‘‘BP n ’’ ($n = 1, 2, 3$), which are listed in Table I. These parameters are specifically chosen for GW signals at various frequency bands that might be probed in future GW experiments. For comparison, we also consider the evolution of DWs without introducing the fermion f , and the corresponding parameter sets with vanishing m_f and y are denoted as ‘‘BP n w/o f ’’ in the following analysis.

In Fig. 1, we present the thermally corrected effective potentials as functions of ϕ/v_ϕ with various temperatures for BP1. The shapes of the potentials for other BPs are similar. The curves are almost identical to the ones obtained with the same λ_ϕ and v_ϕ but without the fermion and the potential bias, and the height of the two local minima of the potential is almost the same. This is because the \mathbb{Z}_2 -violating couplings y and μ_3 are chosen to be small so that they barely affect the phase transition and that the discrete symmetry is only weakly broken.

TABLE I. A list of benchmark points of the model.

	v_ϕ [GeV]	μ_3/v_ϕ	λ_ϕ	y	m_f/v_ϕ
BP1	2×10^9	-10^{-17}	0.1	2.5×10^{-5}	4×10^{-5}
BP2	5×10^4	-10^{-27}	0.1	-9×10^{-8}	10^{-7}
BP3	1.5×10^{11}	-1.2148×10^{-13}	0.1	3×10^{-4}	4×10^{-4}

FIG. 1. Thermally corrected effective potential as functions of ϕ/v_ϕ with various temperatures for BP1.

The tiny potential energy difference V_{bias} between the two local minima plays a crucial role in the evolution of DWs but not in the phase transition.

As shown in Fig. 1, at high temperatures $T \gg v_\phi$, the thermal correction V_T dominates and the total effective potential V has a minimum at $\phi \simeq 0$, indicating a phase that is approximately symmetric under $\phi \leftrightarrow -\phi$. As the temperature declines, the relative importance of V_0 increases and it eventually dominates the effective potential, resulting in two local minima corresponding to a phase where the approximate \mathbb{Z}_2 symmetry is spontaneously broken. At low temperatures $T \ll v_\phi$, the locations of the minima tend towards their values at zero temperature, $\phi_\pm \simeq \pm v_\phi$, where ϕ_- is the false vacuum and ϕ_+ is the true vacuum. According to the curves in Fig. 1, the critical temperature T_c , at which the potential develops two local minima, is $\sim 2v_\phi$, almost the same as that obtained without the \mathbb{Z}_2 -violating terms.

III. EVOLUTION OF DOMAIN WALLS

In the early universe after the phase transition, the field values of ϕ in causally unconnected regions may lie in different local minima of the effective potential. A domain wall would appear

at the boundary separating two regions with different VEVs. Because of the potential bias

$$V_{\text{bias}}(T) \equiv V(\phi_-, T) - V(\phi_+, T) \quad (9)$$

between the false vacuum ϕ_- and the true vacuum ϕ_+ , the probability p_- of the scalar field ϕ being in ϕ_- after the phase transition is different from the probability $p_+ = 1 - p_-$ of being in ϕ_+ . The ratio of the two is [29, 31]

$$\frac{p_-}{p_+} = e^{-\Delta F/T}, \quad (10)$$

where ΔF is the difference between the free energies of the two minima, estimated as $\Delta F \simeq V(\phi_-, T)\xi_-^3 - V(\phi_+, T)\xi_+^3$, and ξ_{\pm} are the correlation lengths of ϕ approximately evaluated by $\xi_{\pm}^{-2} \simeq \partial^2 V(\phi_{\pm}, T)/\partial\phi^2$ [21]. For a large cluster of false vacua to appear in the early universe, p_- needs to be greater than a critical value $p_c \simeq 0.311$ according to the percolation theory [38, 46]. This criterion is easily maintained in this work because the small \mathbb{Z}_2 -violating couplings keep $\Delta F \ll T$ around the critical temperature. Specifically, we have also numerically verified that all the BPs in Table 1 satisfy the condition of $0.311 < p_- \leq 0.5$.

To estimate the evolution of a DW, we numerically calculate the wall tension, i.e., the energy per unit area, by solving the equation of motion (EOM) of ϕ in the static condition. We will show that within the parameter space of interest, the corrections to the tension by the \mathbb{Z}_2 -violating terms are negligible. For a simple evaluation, we consider an instantaneously stable (T -fixed) planar wall invariant in the yz -plane so that the DW configuration is described by $\phi(x, T)$. The DW interpolates the two different minima at $x \rightarrow \pm\infty$. The EOM of $\phi(x, T)$ becomes [24]

$$\frac{\partial^2 \phi(x, T)}{\partial x^2} - \frac{\partial V(\phi, T)}{\partial \phi} = 0, \quad (11)$$

with boundary conditions $\phi(\pm\infty, T) = \phi_{\pm}(T)$, where $\phi_+(T)$ and $\phi_-(T)$ are the true and false vacua at temperature T , respectively. For numerical calculation in practice, we set the boundary at $x_{\pm} = \pm 20/v_{\phi}$ to obtain monotonic solutions corresponding to one domain wall. We have verified that the obtained DW tension is rather insensitive to this choice.

The energy density of the solution,

$$\rho_{\text{DW}} = \frac{1}{2} |\nabla\phi|^2 + V(\phi, T) - V_{\text{min}}(\phi, T), \quad (12)$$

has a peak at x_{peak} , which is taken as the center of the DW. The thickness of DW is approximately $\delta \sim (\sqrt{2\lambda_{\phi}}v_{\phi})^{-1}$ [24], and δ is just a small portion of $(x_+ - x_-)$. Thus, between x_- and x_+ , there are a thin region of the DW and large regions of the two vacua. To avoid counting the false vacuum energy when calculating the tension of the DW, we introduce two boundary points δ_{\pm} between x_{\pm} and x_{peak} to isolate the DW. Specifically, we define δ_{\pm} with the condition,

$$\frac{\rho_{\text{DW}}(x_{\text{peak}}) - \rho_{\text{DW}}(\delta_{\pm})}{\rho_{\text{DW}}(x_{\text{peak}}) - \rho_{\text{DW}}(x_{\pm})} = 0.99 \quad (x_- < \delta_- < x_{\text{peak}} < \delta_+ < x_+). \quad (13)$$

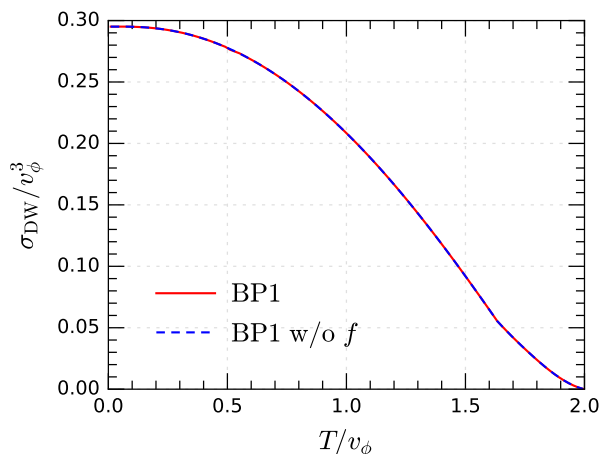


FIG. 2. DW tension varying with temperature. The solid red line and dashed blue line correspond to BP1 with and without the fermion f , respectively.

Accordingly, the DW tension is evaluated as

$$\sigma_{\text{DW}}(T) = \int_{\delta_-}^{\delta_+} \rho_{\text{DW}}(x, T) dx. \quad (14)$$

Figure 2 shows the obtained DW tension σ_{DW} as a function of the temperature for BP1 with and without coupling to the fermion. The \mathbb{Z}_2 -violating couplings y and μ_3 have little influence on σ_{DW} because of their tiny values. After the phase transition, σ_{DW} grows from zero towards $2\sqrt{2\lambda_\phi}v_\phi^3/3$ at low temperatures, resembling the evolution of a DW with a \mathbb{Z}_2 -symmetric potential [24]. The tensions obtained for other BPs have similar features because of the small y and μ_3 .

Once formed, the DW network evolves towards the scaling regime, in which various length scales, such as the typical radius of curvature R_{DW} of the walls and the average distance between the walls, are comparable to the Hubble radius. As a result, one has $R_{\text{DW}} \simeq t/\mathcal{A} \sim (\mathcal{A}H)^{-1}$ [26, 29, 36, 47–49], and the energy density of the DWs can be expressed as

$$\rho_{\text{DW}} = \frac{\mathcal{A}\sigma_{\text{DW}}}{t}, \quad (15)$$

where the parameter $\mathcal{A} \simeq 0.8$ is determined by field theoretic simulation [36] and is almost constant in the scaling regime. We assume that the DW network evolves and eventually collapses in the radiation-dominated era, so the Hubble rate is given by [50]

$$H(T) = \sqrt{\frac{4\pi^3 G g_*(T)}{45}} T^2, \quad (16)$$

with $G \simeq 6.7 \times 10^{-39} \text{ GeV}^{-2}$ [51] the Newtonian gravitational constant and g_* the number of relativistic degrees of freedom [50, 52].

Multiple counteracting forces contribute to the evolution of a DW. The expansion of a DW

is driven by the tension force per unit area,

$$p_T \sim \frac{\sigma_{\text{DW}}}{R_{\text{DW}}} \simeq \rho_{\text{DW}}. \quad (17)$$

When the potential bias is small, σ_{DW} is mainly determined by the \mathbb{Z}_2 -symmetric part of the scalar potential and is nearly constant at low temperatures, so that $p_T \propto T^2$ in the scaling regime for $T \ll v_\phi$ during the radiation-dominated era. The potential bias V_{bias} provides a pressure,

$$p_V \sim V_{\text{bias}}, \quad (18)$$

that collapses the wall. The friction force per unit area F_f exerted by the particles in the ambient environment, which are the f fermions in this work, opposes the motion of the wall [24, 37, 53, 54]. The DW network starts to collapse at the annihilation temperature T_{ann} when

$$p_V + F_f \simeq p_T. \quad (19)$$

The interaction between the DW and the f particles in the thermal bath induces friction on the wall as it moves in the plasma. To estimate the friction, we consider the EOM of the fermion f ,

$$\left[\partial^2 + (m_f + y\phi)^2 \right] f(\mathbf{x}, t) = 0. \quad (20)$$

We begin with estimating the relative motion between a Dirac fermion f and a DW in the DW rest frame with the DW configuration $\phi(x, T)$ discussed in Eq. (11). The fermion wave function has the form $f(\mathbf{x}, t) = g(x) e^{i(-\omega t + p_y y + p_z z)}$. Substituting it into Eq. (20), we obtain

$$\frac{d^2 g(x)}{dx^2} + p_x^2 g(x) - U[\phi(x)] g(x) = 0, \quad (21)$$

where $p_x^2 = \omega^2 - p_y^2 - p_z^2 - m^2$ and $U(\phi) = 2ym_f\phi + y^2\phi^2$. For $p_x \ll \delta^{-1}$ with $\delta \sim (\sqrt{2\lambda_\phi} v_\phi)^{-1}$ the thickness of the wall [24], this collision problem can be approximated by the classic one-dimensional scattering of a free particle by a step potential, with $\phi(x)$ approximated as

$$\phi(x) \simeq \begin{cases} \phi_- & (x < x_{\text{peak}}), \\ \phi_+ & (x > x_{\text{peak}}), \end{cases} \quad (22)$$

recalling that we have chosen the coordinate so that the true (false) vacuum lies at $x > 0$ ($x < 0$). For a fermion traveling from a vacuum ϕ_i to another vacuum ϕ_j , the probability of it being

reflected by the DW is

$$R_{\phi_i \rightarrow \phi_j} \simeq \begin{cases} \frac{[U(\phi_i) - U(\phi_j)]^2}{[\sqrt{p_x^2 - U(\phi_i)} + \sqrt{p_x^2 - U(\phi_j)}]^4}, & p_x^2 \geq \max\{U(\phi_i), U(\phi_j)\}, \\ 1, & U(\phi_i) \leq p_x^2 < U(\phi_j), \end{cases} \quad (23)$$

where $\phi_{i/j} = \phi_{+/-}$ or $\phi_{-/+}$. Note that values of p_x outside the ranges quoted in Eq. (23) correspond to bound state solutions and are irrelevant to the calculation of friction. The actual reflectivity of f is generally smaller than that obtained with this approximation because the DW configuration $\phi(x)$ is gentler than a steep step, and so is $U[\phi(x)]$.

DWs expand after formation with an average velocity v_{DW} . To estimate the friction force, we consider a DW moving along the x -axis at velocity v_{DW} . According to the convention above, v_{DW} is positive when the DW moves from the false vacuum to the true one. For a fermion f in the thermal bath with momentum p , its velocity relative to the DW is $(p_x - \omega v_{\text{DW}})/(\omega - p_x v_{\text{DW}})$, and the momentum transfer in a collision with the wall is $-2(p_x - \omega v_{\text{DW}})/(1 - v_{\text{DW}}^2)$. Therefore, the friction force per unit area exerted on the DW is [21, 24, 37, 50]

$$F_f = \frac{2}{\pi^2} \frac{1}{1 - v_{\text{DW}}^2} \int_0^{+\infty} \int_{-\infty}^{+\infty} R(p_x) \frac{(p_x - \omega v_{\text{DW}})^2}{\omega - p_x v_{\text{DW}}} \frac{1}{e^{\omega/T} + 1} p_{\perp} dp_x dp_{\perp}, \quad (24)$$

where $p_{\perp} \equiv \sqrt{p_y^2 + p_z^2}$, and the reflection probability $R(p_x)$ is defined as

$$R(p_x) = \begin{cases} R_{\phi_+ \rightarrow \phi_-} & (p_x < p_0), \\ -R_{\phi_- \rightarrow \phi_+} & (p_x > p_0), \end{cases} \quad (25)$$

where $p_0 = v_{\text{DW}} \sqrt{(p_{\perp}^2 + m^2)/(1 - v_{\text{DW}}^2)}$, and $p_x = p_0$ indicates that the fermion is at rest with respect to the wall.

Before proceeding to the numerical results, we present qualitative¹ estimates for the more analytically calculable regime of $v_{\phi} \gg T \gg m_f \gg |yv_{\phi}|$, where the phase transition has settled while the temperature remains high enough to keep the fermions in the thermal bath. The limit $m_f \gg |yv_{\phi}|$ allows us to treat \mathbb{Z}_2 -violating effects as perturbations. The results for the limit $m_f \ll |yv_{\phi}|$ share the same qualitative behavior to be discussed below.

In this limit with a sufficient small μ_3 , the dominant thermal correction to the effective potential comes from the fermions in the thermal bath, so that the thermal contribution to V_{bias} is roughly $\Delta V_{\text{T}} \equiv V_{\text{T}}(\phi_-, T) - V_{\text{T}}(\phi_+, T) \sim yv_{\phi} m_f T^2$. The friction can be estimated as $F_f \sim n_f \Delta p R \sim T^4 v_{\text{DW}} R$, where Δp is the momentum exchange and n_f is the number density of the fermions. The scaling of the reflection probability can be estimated according to Eq. (23), $R \sim (yv_{\phi})^2 m_f^2 / \omega^4$, with the typical particle energy $\omega \sim T$. Therefore, the friction is negligible in this limit compared to the pressure, $F_f \ll \Delta V_{\text{T}} < V_{\text{bias}} \sim p_V$. The DWs thus collapse at the time when $p_V / p_{\text{T}} \gtrsim 1$.

¹ In the following qualitative estimates, we ignore numerical factors and only consider the scaling behavior.

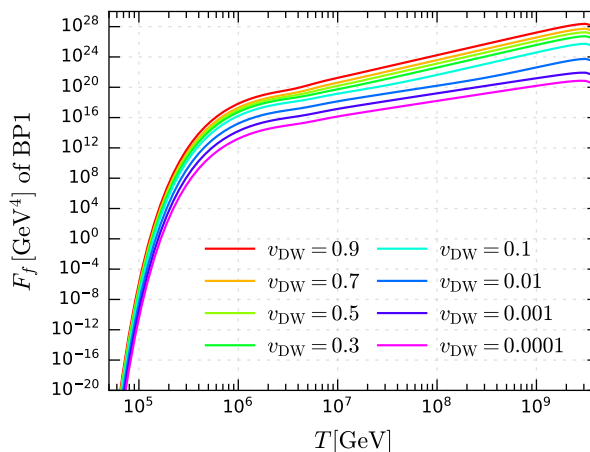


FIG. 3. Friction force per unit area F_f exerted on the DW as a function of the temperature with various wall velocities v_{DW} for BP1.

If $V_{\text{bias}}(T=0) \gg \Delta V_{\text{T}}$, V_{bias} is dominated by the asymmetric terms in the zero-temperature scalar potential, which are independent of the temperature. This reduces to the conventional scenario studied extensively in the literature without the background fermionic thermal bath. On the other hand, if $V_{\text{bias}}(T=0) \ll \Delta V_{\text{T}}$ before the DW network collapses, V_{bias} and thus the pressure is mainly determined by the thermal correction by the fermions, which translates to $p_{\text{V}}/p_{\text{T}} \sim \Delta V_{\text{T}}/p_{\text{T}} \sim |yv_{\phi}|m_f M_{\text{P}}/\sigma_{\text{DW}}$ according to Eqs. (16), (17), and (18), where M_{P} is the Planck mass. In this case, $p_{\text{V}}/p_{\text{T}}$ is almost temperature-independent for $m_f \ll T \ll v_{\phi}$.

If $|yv_{\phi}|m_f M_{\text{P}} \gg \sigma_{\text{DW}}$, the thermal correction renders the DWs unstable right after they are formed, and they may not evolve into the scaling regime. Therefore, it is important to examine the size of the thermal correction to V_{bias} for the evolution of the DWs. If $|yv_{\phi}|m_f M_{\text{P}} \ll \sigma_{\text{DW}}$, the thermal effect alone is too weak to make the DWs collapse, and the evolution is again determined by the temperature-independent part $V_{\text{bias}}(T=0)$. For the intermediate regime between the two extremes, the thermal correction is small enough to keep the DW network metastable so that it evolves into the scaling regime, while large enough to compete with $V_{\text{bias}}(T=0)$ to affect the late time evolution and its accompanying phenomenology. However, it is no longer easy to estimate the results analytically. The BPs fall within this regime and we present their numerical results in the following.

In Fig. 3, we plot the friction F_f on the DW as a function of the temperature with various wall velocities v_{DW} for BP1. The frictions evaluated for other BPs share a similar behavior qualitatively. At high temperatures close to the critical temperature of the phase transition, the calculated friction falls drastically because of the shallower potential difference between the true and false vacua, reducing the reflection probability of the incoming fermion to the wall. At low temperatures, F_f decreases exponentially due to the Boltzmann suppression when the temperature becomes comparable to the fermion mass. For smaller v_{DW} , the friction F_f decreases slowly due to the smaller momentum transfer per collision between the wall and the fermion. For simplicity, we will assume the typical velocity $v_{\text{DW}} \simeq 0.3$ [55, 56] for the rest of

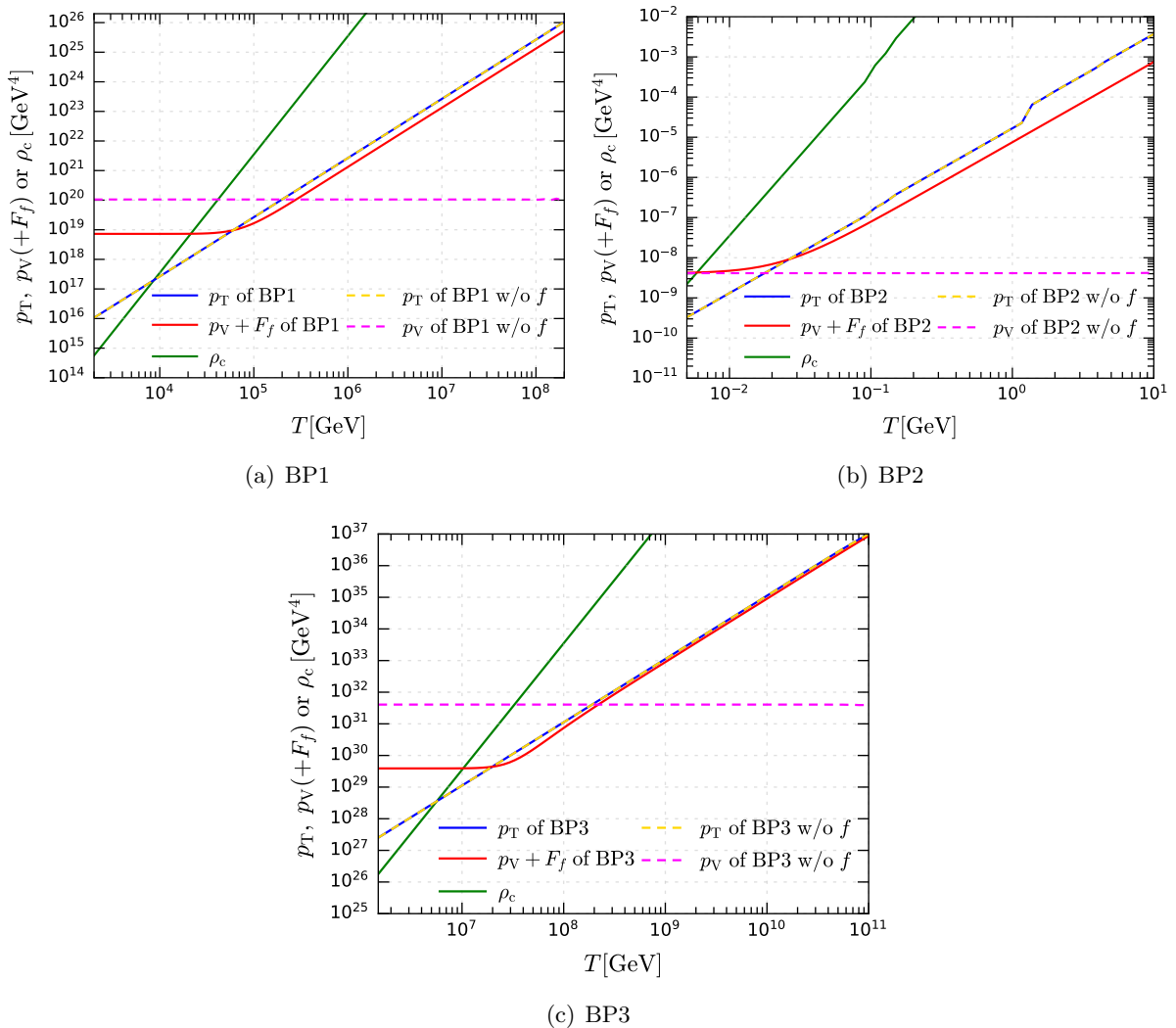


FIG. 4. p_T , $p_V + F_f$, p_V , and ρ_c as functions of the temperature T for the three BPs. The solid (dashed) lines correspond to the result with (without) the fermion f .

this work.

As the universe expands, the energy density of the DWs in the scaling regime dilutes slower than those of matter and radiation. If the DW network collapses late, they could dominate the energy density of the universe at the temperature T_{dom} corresponding to [29, 31, 36–38]

$$p_T \sim \mathcal{A} \sigma_{\text{DW}} H \sim \rho_{\text{DW}} \simeq \rho_c = \frac{3H^2}{8\pi G}, \quad (26)$$

where ρ_c is the critical density. For a consistent cosmological history, the DWs need to collapse before they overclose the universe. This sets the condition $T_{\text{ann}} > T_{\text{dom}}$, which is equivalent to $p_T \lesssim \rho_c$ at T_{ann} .

In Fig. 4, we summarize all the previous considerations on the evolution and the collapse of DWs by plotting p_T , $p_V(+F_f)$, and ρ_c as functions of the temperature for the three BPs. For each BP, the two curves for the tension force p_T with and without the fermion overlap with

TABLE II. Values of T_{ann} , f_{peak} , and $\Omega_{\text{GW}}(f_{\text{peak}})h^2$ for the BPs.

	T_{ann} [GeV]	f_{peak} [Hz]	$\Omega_{\text{GW}}(f_{\text{peak}})h^2$
BP1	6.02×10^4	1.00×10^{-2}	5.77×10^{-10}
BP1 w/o f	2.00×10^5	3.32×10^{-2}	4.77×10^{-12}
BP2	2.62×10^{-2}	2.98×10^{-9}	8.36×10^{-11}
BP2 w/o f	1.77×10^{-2}	2.01×10^{-9}	4.01×10^{-10}
BP3	1.98×10^7	3.30	8.77×10^{-9}
BP3 w/o f	1.90×10^8	3.17×10^1	1.02×10^{-12}

each other, because the DW tensions are almost unaltered by the small Yukawa coupling, as shown in Fig. 2. After the phase transition, the p_T curves in the three BPs decrease with the temperature as T^2 during the radiation-dominated era according to Eq. (17). The step-like features at $T \sim \text{GeV}$ and $T \sim 10^{-1} \text{ GeV}$ for BP2 are caused by the thresholds in the effective degrees of freedom $g_*(T)$.

In the temperature ranges shown in Fig. 4, the calculated friction F_f with $v_{\text{DW}} = 0.3$ for the three BPs are always negligible, compared to p_V . Since the μ_3 values in the BPs are extremely small, the thermal correction to p_V induced by μ_3 is insignificant, compared to the thermal correction from the Yukawa coupling, which renders $p_V \propto T^2$ at high temperatures. Therefore, all the curves of $p_V + F_f$ in the three BPs are basically parallel to p_T at high temperatures. At low temperatures $T \lesssim |M_f(v_\phi)|$, the potential bias induced by thermal corrections becomes negligible and the curves of $p_V (+F_f)$ become flat. Here, the differences between BP n and BP n w/o f are caused by the Coleman-Weinberg effective potential V_{CW} .

The DW annihilation temperature T_{ann} is determined by the intersection between the curves of $p_V(+F_f)$ and p_V , and the obtained T_{ann} values for the BPs are given in Table II. For the results with the fermion f shown in Fig. 4, the p_T curves intersect with the $p_V + F_f$ curves at which the $p_V + F_f$ curves start to rise with T , indicating that the thermal corrections are getting important. Since the p_T and $p_V + F_f$ curves are parallel to each other at high temperatures, their intersection points, and thus T_{ann} , are rather sensitive to increasing values of $|y|$ and $|m_f|$. For BP1 and BP3, the DWs collapse later with lower T_{ann} than their counterpart without the fermion, affected mainly by the differences in the Coleman-Weinberg effective potential V_{CW} . Whilst for BP2, the correction by V_{CW} is almost negligible. The earlier collapse time of the DWs in BP2 relative to that without the fermion is driven by the thermal correction from the fermion.

Finally, if the DWs do not collapse, they dominate the early universe at the temperature T_{dom} , which is determined by the intersection between the curves of p_T and ρ_c . In all the BPs, the annihilation temperatures T_{ann} are higher than both T_{dom} and the big bang nucleosynthesis temperature $\sim 1 \text{ MeV}$ [50, 51], indicating a consistent cosmological history.

IV. SPECTRUM OF GRAVITATIONAL WAVES

The DW network undergoes dynamical evolution from its initial formation to eventual collapse, and a portion of its energy density would be radiated as GWs. A rough estimate of the energy density of the emitted GWs can be obtained by the quadrupole approximation, where the quadrupole moment of the DWs is evaluated by $Q_{ij} \sim \mathcal{A}\sigma_{\text{DW}}t^4$ in the scaling regime. Thus, the power of gravitational radiation is estimated as $P \sim G\ddot{Q}_{ij}(t)\ddot{Q}_{ij}(t) \sim G\mathcal{A}^2\sigma_{\text{DW}}^2t^2$, and the GW energy density is given by $\rho_{\text{GW}} \sim Pt/t^3 \sim G\mathcal{A}^2\sigma_{\text{DW}}^2$ [57, 58]. Although such an estimate may not be accurate, it reveals that the GW energy density generated by DWs is basically proportional to $G\mathcal{A}^2\sigma_{\text{DW}}^2$.

The SGWB produced by collapsing DWs has been evaluated via numerical simulations [29, 30, 36, 38, 59, 60]. The frequency spectrum of the SGWB is commonly represented by a dimensionless quantity

$$\Omega_{\text{GW}}(f) \equiv \frac{1}{\rho_c} \frac{d\rho_{\text{GW}}}{d \ln f}, \quad (27)$$

where f is the GW frequency. Previous research indicates that the majority of GWs emitted from DWs is at a peak frequency $f_{\text{peak}}(T_{\text{ann}}) \sim H(T_{\text{ann}})$, corresponding to the time when DWs collapse at the annihilation temperature T_{ann} . Taking into account the cosmological redshift, the peak frequency today becomes [29, 36]

$$f_{\text{peak}}(T_0) = \frac{a(T_{\text{ann}})H(T_{\text{ann}})}{a(T_0)} = \left[\frac{g_{*S}(T_0)}{g_{*S}(T_{\text{ann}})} \right]^{1/3} \frac{T_0 H(T_{\text{ann}})}{T_{\text{ann}}}, \quad (28)$$

where $a(T)$ is the scale factor at temperature T , $T_0 = 2.7255$ K is the present temperature of the universe, and $g_{*S}(T)$ is the number of entropic relativistic degrees of freedom [50, 52]. We set $g_{*S}(T_{\text{ann}} \gtrsim 100 \text{ GeV}) \simeq 100$ and $g_{*S}(T_0) = 3.91$.

The peak amplitude of $\Omega_{\text{GW}}(f)$ at the annihilation temperature is [29, 36]

$$\Omega_{\text{GW}}(f_{\text{peak}})|_{T_{\text{ann}}} = \frac{8\pi\tilde{\epsilon}_{\text{GW}}G^2\mathcal{A}^2\sigma_{\text{DW}}^2(T_{\text{ann}})}{3H^2(T_{\text{ann}})}, \quad (29)$$

where $\tilde{\epsilon}_{\text{GW}} = 0.7$ is a factor determined by numerical simulations [36]. Taking account of the cosmic expansion, the peak amplitude at the present can be expressed as [38]

$$\Omega_{\text{GW}}(f_{\text{peak}})|_{T_0} = \Omega_{\text{rad}}(T_0) \frac{g_*(T_{\text{ann}})}{g_*(T_0)} \left[\frac{g_{*S}(T_0)}{g_{*S}(T_{\text{ann}})} \right]^{\frac{4}{3}} \Omega_{\text{GW}}(f_{\text{peak}})|_{T_{\text{ann}}}, \quad (30)$$

where $\Omega_{\text{rad}}(T_0) = 1.68 \times 5.38 \times 10^{-5}$ is the fraction of the radiation energy density today [51] and we adopt $g_*(T_{\text{ann}} \gtrsim 100 \text{ GeV}) \simeq 100$ and $g_*(T_0) = 3.36$. Furthermore, causality implies $\Omega_{\text{GW}} \propto f^3$ for $f < f_{\text{peak}}$ [61], while numerical simulations suggest $\Omega_{\text{GW}} \propto f^{-1}$ for $f > f_{\text{peak}}$ [36]².

² Numerical simulations in Refs. [62, 63] yield slightly different spectral indices for $f > f_{\text{peak}}$.

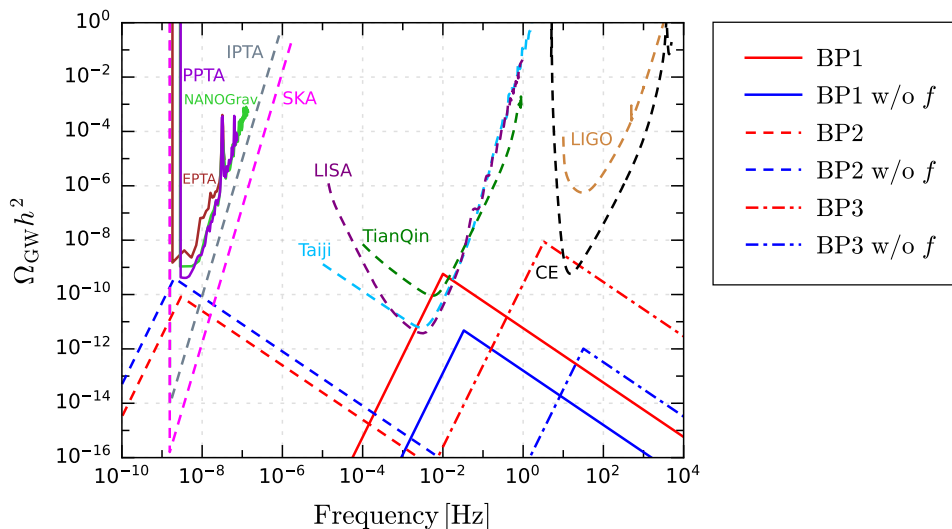


FIG. 5. SGWB spectra induced by the DWs for the three BPs with (red lines) and without (blue lines) the fermion f . Constraints and sensitivity curves of various GW experiments are also plotted.

Therefore, the present SGWB spectrum can be formulated as

$$\Omega_{\text{GW}}(f) = \Omega_{\text{GW}}(f_{\text{peak}})|_{T_0} \times \begin{cases} \left(\frac{f}{f_{\text{peak}}}\right)^3, & f \leq f_{\text{peak}}, \\ \left(\frac{f}{f_{\text{peak}}}\right)^{-1}, & f > f_{\text{peak}}. \end{cases} \quad (31)$$

When comparing with GW experiments, the SGWB spectrum is typically expressed as $\Omega_{\text{GW}} h^2$, where $h = 0.674$ [51] is the Hubble constant in units of $100 \text{ km s}^{-1} \text{ Mpc}^{-1}$.

We evaluate the SGWB spectra induced by the DWs for the three BPs with and without the fermion, and the obtained peak frequencies and peak amplitudes are listed in Table II. The SGWB spectra as functions of GW frequency are demonstrated in Fig. 5, where the constraints and sensitivities curves of current and future GW experiments are also presented.

For BP1 without the fermion, the peak GW frequency is estimated to be $3.32 \times 10^{-2} \text{ Hz}$ with a peak GW amplitude of $\Omega_{\text{GW}}(f_{\text{peak}})h^2 \simeq 4.77 \times 10^{-12}$. Nevertheless, including the fermion in BP1 would decrease both the DW annihilation temperature T_{ann} and the peak frequency f_{peak} by a factor of ~ 3.3 , increasing the peak amplitude by two orders of magnitude. As a result, future space-borne GW experiments, such as Laser Interferometer Space Antenna (LISA) [12], TianQin [14], and Taiji [13], have larger probabilities of probing the latter scenario.

Furthermore, BP2 with or without the fermion predicts a peak frequency around nHz, which falls within the sensitive band of PTA experiments, including the North American Nanohertz Observatory for Gravitational Waves (NANOGrav) [7], the European Pulsar Timing Array (EPTA) [8], the Parkes Pulsar Timing Array (PPTA) [9], the International Pulsar Timing Array (IPTA) [10], and the Square Kilometer Array (SKA) [11]. Compared to BP2 without f , BP2 exhibits a reduction in the peak amplitude by a factor of ~ 4.8 , due to a slightly lower

DW annihilation temperature. The predicted GW spectra from both cases remain consistent with the current constraints imposed by NANOGrav, EPTA, and PPTA, while future IPTA and SKA experiments could easily test these scenarios.

Finally, BP3 without the fermion leads to $f_{\text{peak}} \simeq 31.7$ Hz, which lies within the sensitive band of ground-based GW experiments, such as the Laser Interferometer Gravitational Wave Observatory (LIGO), Virgo, KAGRA [5], and the Cosmic Explorer (CE) [6]. However, the predicted peak amplitude $\Omega_{\text{GW}}(f_{\text{peak}})h^2 \simeq 1.02 \times 10^{-12}$ is too low to be probed in these experiments. Nonetheless, when the effect of the fermion is included, the peak amplitude increases to 8.77×10^{-9} , which is promising to be detected by the future CE experiment. Because of $H \propto T^2$ at the radiation-dominated era, a decrease of T_{ann} by one order of magnitude would reduce $H(T_{\text{ann}})$ by two orders of magnitude and hence increase $\Omega_{\text{GW}}(f_{\text{peak}})|_{T_{\text{ann}}}$ by four orders of magnitude according to Eq. (29). This explains the great difference between the GW spectra of BP3 and BP3 w/o f .

Below, we investigate how the VEV v_ϕ affects the results. As v_ϕ varies, the curves of p_T in Fig. 4 would shift compared to those of $p_V + F_f$, leading to modifications in the DW annihilation temperature T_{ann} , which consequently affect both f_{peak} and $\Omega_{\text{GW}}(f_{\text{peak}})h^2$. Based on the BPs listed in Table I, we vary the value of v_ϕ while keeping the rest parameters λ_3/v_ϕ , λ_ϕ , y , and m_f/v_ϕ unchanged, and show T_{ann} , f_{peak} , and $\Omega_{\text{GW}}(f_{\text{peak}})h^2$ as functions of v_ϕ in Fig. 6. The red curves, corresponding to the scenario including the fermionic effects, display clear initial points. This is because if v_ϕ is too small, the resulting p_T in the scaling regime would fall below $p_V + F_f$ at all temperatures, and the DW annihilation temperature T_{ann} would not exist. In this case, actually, the DWs would collapse rapidly before entering the scaling regime, and their energy density would be insufficient to generate significant GW signals. On the other hand, the blue curves for the scenarios without the fermion extend to lower values of v_ϕ , because p_V is independent of the temperature, ensuring the existence of T_{ann} .

For large values of v_ϕ in the scenario with the fermion, T_{ann} is determined at low temperatures where p_V is basically temperature-independent, similar to the scenario without the fermion. Consequently, the values of T_{ann}/v_ϕ in both scenarios tend to be constant for large v_ϕ , and their difference comes from the fermionic contribution to the potential bias in V_{CW} . Since f_{peak} is positively correlated with T_{ann} , a constant T_{ann}/v_ϕ implies that f_{peak} is also positively correlated with v_ϕ , as shown in the middle column of Fig. 6 for large v_ϕ . Furthermore, because an increase in v_ϕ would enhance the DW tension σ_{DW} , $\Omega_{\text{GW}}(f_{\text{peak}})h^2$ demonstrates a significant and consistent increase with v_ϕ in all considered scenarios.

V. SUMMARY

In this paper, we study the evolution of collapsing domain walls affected by the thermal corrections from matter particles and explore the impact on the induced gravitational waves. We begin by considering a simple model with a real scalar field ϕ coupled to a Dirac spinor field f . The scalar potential is assumed to respect an approximate \mathbb{Z}_2 symmetry, which is slightly

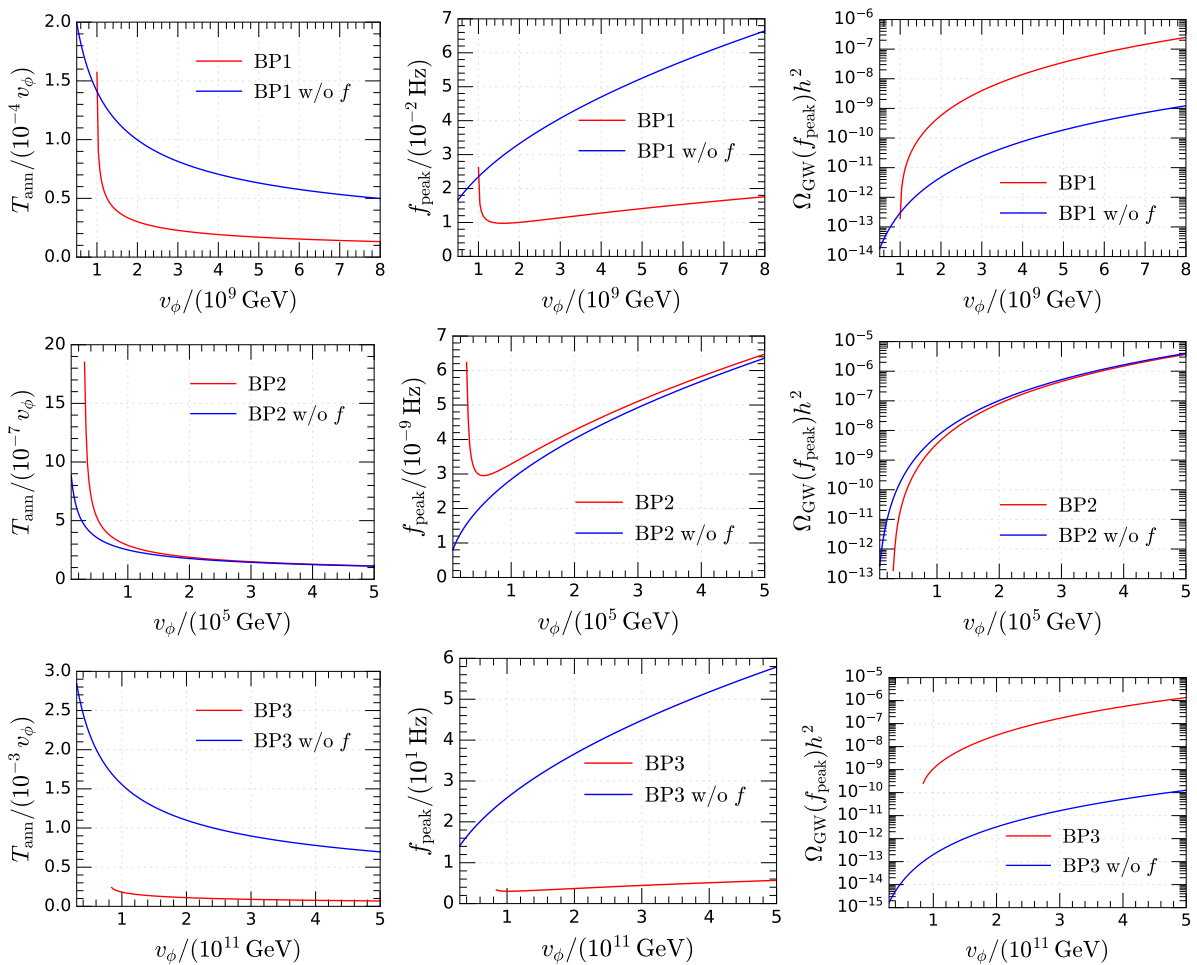


FIG. 6. T_{ann}/v_ϕ , $\Omega_{\text{GW}}(f_{\text{peak}})h^2$, and f_{peak} as functions of v_ϕ , with the other parameters fixed as in the three BPs. The left, middle, and right columns correspond to BP1, BP2, and BP3, respectively. The red and blue curves denote the results for the cases with and without the fermion, respectively.

violated by a ϕ^3 term at the tree level and by the Yukawa coupling between ϕ and f at the one-loop level. The \mathbb{Z}_2 symmetry results in DWs generated after a second-order phase transition via the Kibble mechanism, while the potential bias V_{bias} between the true and false vacua arising from the \mathbb{Z}_2 -violating terms provides a pressure $p_V \sim V_{\text{bias}}$ that drives the collapse of DWs.

In contrast to previous studies that only consider a temperature-independent bare V_{bias} , we incorporate both quantum and thermal corrections arising from the Yukawa coupling with a fermion field to investigate the temperature dependence of V_{bias} and its influences. After constructing the effective potential with zero-temperature Coleman-Weinberg corrections and finite-temperature corrections at the one-loop level, we systematically compute the temperature dependence of key physical quantities for the evolution of DWs, including the DW tension σ_{DW} , the tension force p_T , the pressure p_V , and the friction force F_f . The Coleman-Weinberg potential contributed by the Yukawa coupling shifts the temperature-independent part of V_{bias} . On the other hand, because of the thermal corrections from the fermion, the pressure p_V is proportional to T^2 at sufficiently high temperatures, leading to further differences in the deter-

mined DW annihilation temperature T_{ann} between the scenarios with and without the fermionic contribution.

The frequency spectra of the SGWB generated by collapsing DWs in three BPs are further estimated, and we find that the differences in T_{ann} could lead to substantial modifications in the GW spectra. For the selected parameter sets, the GW spectra corresponding to BP1, BP2, and BP3 lie within the observational windows of space-borne interferometers, PTAs, and ground-based interferometers, respectively. Therefore, these characteristic spectral modifications could potentially be verified by future GW experiments. Remarkably, the DW annihilation temperature for BP3 decreases by a factor of 10 compared to the case without the fermionic contributions, leading to a dramatic enhancement in the peak amplitude of the GW spectrum by four orders of magnitude, which significantly improves the detectability prospects in future GW experiments. Moreover, we investigate the dependence of T_{ann} , f_{peak} , and $\Omega_{\text{GW}}(f_{\text{peak}})h^2$ on the VEV v_ϕ , revealing that increasing v_ϕ would significantly enhance the amplitude of the GW spectrum.

ACKNOWLEDGMENTS

This work is supported by the Guangzhou Science and Technology Planning Project under Grant No. 2024A04J4026.

-
- [1] **LIGO Scientific, Virgo** Collaboration, B. P. Abbott *et al.*, “Observation of Gravitational Waves from a Binary Black Hole Merger,” *Phys. Rev. Lett.* **116** (2016) 061102, [arXiv:1602.03837 \[gr-qc\]](#).
 - [2] **LIGO Scientific, Virgo** Collaboration, B. P. Abbott *et al.*, “GW170817: Observation of Gravitational Waves from a Binary Neutron Star Inspiral,” *Phys. Rev. Lett.* **119** (2017) 161101, [arXiv:1710.05832 \[gr-qc\]](#).
 - [3] C. Caprini and D. G. Figueroa, “Cosmological Backgrounds of Gravitational Waves,” *Class. Quant. Grav.* **35** (2018) 163001, [arXiv:1801.04268 \[astro-ph.CO\]](#).
 - [4] A. I. Renzini, B. Goncharov, A. C. Jenkins, and P. M. Meyers, “Stochastic Gravitational-Wave Backgrounds: Current Detection Efforts and Future Prospects,” *Galaxies* **10** (2022) 34, [arXiv:2202.00178 \[gr-qc\]](#).
 - [5] **KAGRA, LIGO Scientific, Virgo, VIRGO** Collaboration, B. P. Abbott *et al.*, “Prospects for observing and localizing gravitational-wave transients with Advanced LIGO, Advanced Virgo and KAGRA,” *Living Rev. Rel.* **21** (2018) 3, [arXiv:1304.0670 \[gr-qc\]](#).
 - [6] **LIGO Scientific** Collaboration, B. P. Abbott *et al.*, “Exploring the Sensitivity of Next Generation Gravitational Wave Detectors,” *Class. Quant. Grav.* **34** (2017) 044001, [arXiv:1607.08697 \[astro-ph.IM\]](#).
 - [7] **NANOGrav** Collaboration, Z. Arzoumanian *et al.*, “The NANOGrav 11-year Data Set: Pulsar-timing Constraints On The Stochastic Gravitational-wave Background,” *Astrophys. J.* **859** (2018) 47, [arXiv:1801.02617 \[astro-ph.HE\]](#).
 - [8] L. Lentati *et al.*, “European Pulsar Timing Array Limits On An Isotropic Stochastic

- Gravitational-Wave Background,” *Mon. Not. Roy. Astron. Soc.* **453** (2015) 2576–2598, [arXiv:1504.03692 \[astro-ph.CO\]](#).
- [9] R. M. Shannon *et al.*, “Gravitational waves from binary supermassive black holes missing in pulsar observations,” *Science* **349** (2015) 1522–1525, [arXiv:1509.07320 \[astro-ph.CO\]](#).
- [10] G. Hobbs *et al.*, “The international pulsar timing array project: using pulsars as a gravitational wave detector,” *Class. Quant. Grav.* **27** (2010) 084013, [arXiv:0911.5206 \[astro-ph.SR\]](#).
- [11] G. Janssen *et al.*, “Gravitational wave astronomy with the SKA,” *PoS AASKA14* (2015) 037, [arXiv:1501.00127 \[astro-ph.IM\]](#).
- [12] LISA Collaboration, P. Amaro-Seoane *et al.*, “Laser Interferometer Space Antenna,” [arXiv:1702.00786 \[astro-ph.IM\]](#).
- [13] W.-H. Ruan, Z.-K. Guo, R.-G. Cai, and Y.-Z. Zhang, “Taiji program: Gravitational-wave sources,” *Int. J. Mod. Phys. A* **35** (2020) 2050075, [arXiv:1807.09495 \[gr-qc\]](#).
- [14] Z.-C. Liang, Y.-M. Hu, Y. Jiang, J. Cheng, J.-d. Zhang, and J. Mei, “Science with the TianQin Observatory: Preliminary results on stochastic gravitational-wave background,” *Phys. Rev. D* **105** (2022) 022001, [arXiv:2107.08643 \[astro-ph.CO\]](#).
- [15] NANOGrav Collaboration, G. Agazie *et al.*, “The NANOGrav 15 yr Data Set: Evidence for a Gravitational-wave Background,” *Astrophys. J. Lett.* **951** (2023) L8, [arXiv:2306.16213 \[astro-ph.HE\]](#).
- [16] EPTA, InPTA: Collaboration, J. Antoniadis *et al.*, “The second data release from the European Pulsar Timing Array - III. Search for gravitational wave signals,” *Astron. Astrophys.* **678** (2023) A50, [arXiv:2306.16214 \[astro-ph.HE\]](#).
- [17] D. J. Reardon *et al.*, “Search for an Isotropic Gravitational-wave Background with the Parkes Pulsar Timing Array,” *Astrophys. J. Lett.* **951** (2023) L6, [arXiv:2306.16215 \[astro-ph.HE\]](#).
- [18] H. Xu *et al.*, “Searching for the Nano-Hertz Stochastic Gravitational Wave Background with the Chinese Pulsar Timing Array Data Release I,” *Res. Astron. Astrophys.* **23** (2023) 075024, [arXiv:2306.16216 \[astro-ph.HE\]](#).
- [19] NANOGrav Collaboration, A. Afzal *et al.*, “The NANOGrav 15 yr Data Set: Search for Signals from New Physics,” *Astrophys. J. Lett.* **951** (2023) L11, [arXiv:2306.16219 \[astro-ph.HE\]](#). [Erratum: *Astrophys.J.Lett.* 971, L27 (2024), Erratum: *Astrophys.J.* 971, L27 (2024)].
- [20] EPTA, InPTA Collaboration, J. Antoniadis *et al.*, “The second data release from the European Pulsar Timing Array - IV. Implications for massive black holes, dark matter, and the early Universe,” *Astron. Astrophys.* **685** (2024) A94, [arXiv:2306.16227 \[astro-ph.CO\]](#).
- [21] T. W. B. Kibble, “Topology of Cosmic Domains and Strings,” *J. Phys. A* **9** (1976) 1387–1398.
- [22] A. Vilenkin, “Gravitational Field of Vacuum Domain Walls and Strings,” *Phys. Rev. D* **23** (1981) 852–857.
- [23] T. Vachaspati, “Lectures on cosmic topological defects,” *ICTP Lect. Notes Ser.* **4** (2001) 165–202, [arXiv:hep-ph/0101270](#).
- [24] A. Vilenkin and E. P. S. Shellard, *Cosmic Strings and Other Topological Defects*. Cambridge University Press, 7, 2000.
- [25] Y. B. Zeldovich, I. Y. Kobzarev, and L. B. Okun, “Cosmological Consequences of the Spontaneous Breakdown of Discrete Symmetry,” *Zh. Eksp. Teor. Fiz.* **67** (1974) 3–11.
- [26] W. H. Press, B. S. Ryden, and D. N. Spergel, “Dynamical Evolution of Domain Walls in an Expanding Universe,” *Astrophys. J.* **347** (1989) 590–604.
- [27] L. F. Abbott and M. B. Wise, “Wormholes and Global Symmetries,” *Nucl. Phys. B* **325** (1989) 687–704.
- [28] S. R. Coleman and K.-M. Lee, “Wormholes made without massless matter fields,” *Nucl. Phys. B*

- 329** (1990) 387–409.
- [29] T. Hiramatsu, M. Kawasaki, and K. Saikawa, “Gravitational Waves from Collapsing Domain Walls,” *JCAP* **05** (2010) 032, [arXiv:1002.1555 \[astro-ph.CO\]](#).
- [30] M. Kawasaki and K. Saikawa, “Study of gravitational radiation from cosmic domain walls,” *JCAP* **09** (2011) 008, [arXiv:1102.5628 \[astro-ph.CO\]](#).
- [31] G. B. Gelmini, M. Gleiser, and E. W. Kolb, “Cosmology of Biased Discrete Symmetry Breaking,” *Phys. Rev. D* **39** (1989) 1558.
- [32] K. Kadota, M. Kawasaki, and K. Saikawa, “Gravitational waves from domain walls in the next-to-minimal supersymmetric standard model,” *JCAP* **10** (2015) 041, [arXiv:1503.06998 \[hep-ph\]](#).
- [33] D. Borah and A. Dasgupta, “Probing left-right symmetry via gravitational waves from domain walls,” *Phys. Rev. D* **106** (2022) 035016, [arXiv:2205.12220 \[hep-ph\]](#).
- [34] D. Coulson, Z. Lalak, and B. A. Ovrut, “Biased domain walls,” *Phys. Rev. D* **53** (1996) 4237–4246.
- [35] M. Gleiser and R. Roberts, “Gravitational waves from collapsing vacuum domains,” *Phys. Rev. Lett.* **81** (1998) 5497–5500, [arXiv:astro-ph/9807260](#).
- [36] T. Hiramatsu, M. Kawasaki, and K. Saikawa, “On the estimation of gravitational wave spectrum from cosmic domain walls,” *JCAP* **02** (2014) 031, [arXiv:1309.5001 \[astro-ph.CO\]](#).
- [37] K. Nakayama, F. Takahashi, and N. Yokozaki, “Gravitational waves from domain walls and their implications,” *Phys. Lett. B* **770** (2017) 500–506, [arXiv:1612.08327 \[hep-ph\]](#).
- [38] K. Saikawa, “A review of gravitational waves from cosmic domain walls,” *Universe* **3** (2017) 40, [arXiv:1703.02576 \[hep-ph\]](#).
- [39] Z. Zhang, C. Cai, Y.-H. Su, S. Wang, Z.-H. Yu, and H.-H. Zhang, “Nano-Hertz gravitational waves from collapsing domain walls associated with freeze-in dark matter in light of pulsar timing array observations,” *Phys. Rev. D* **108** (2023) 095037, [arXiv:2307.11495 \[hep-ph\]](#).
- [40] D. Stojkovic, K. Freese, and G. D. Starkman, “Holes in the walls: Primordial black holes as a solution to the cosmological domain wall problem,” *Phys. Rev. D* **72** (2005) 045012, [arXiv:hep-ph/0505026](#).
- [41] D. I. Dunsky, A. Ghoshal, H. Murayama, Y. Sakakihara, and G. White, “GUTs, hybrid topological defects, and gravitational waves,” *Phys. Rev. D* **106** (2022) 075030, [arXiv:2111.08750 \[hep-ph\]](#).
- [42] G. Lazarides and Q. Shafi, “Axion Models with No Domain Wall Problem,” *Phys. Lett. B* **115** (1982) 21–25.
- [43] S. R. Coleman and E. J. Weinberg, “Radiative Corrections as the Origin of Spontaneous Symmetry Breaking,” *Phys. Rev. D* **7** (1973) 1888–1910.
- [44] C. Delaunay, C. Grojean, and J. D. Wells, “Dynamics of Non-renormalizable Electroweak Symmetry Breaking,” *JHEP* **04** (2008) 029, [arXiv:0711.2511 \[hep-ph\]](#).
- [45] M. Quiros, “Finite temperature field theory and phase transitions,” in *ICTP Summer School in High-Energy Physics and Cosmology*, pp. 187–259. 1, 1999, [arXiv:hep-ph/9901312](#).
- [46] D. Stauffer, “Scaling theory of percolation clusters,” *Phys. Rept.* **54** (1979) 1–74.
- [47] M. Hindmarsh, “Analytic scaling solutions for cosmic domain walls,” *Phys. Rev. Lett.* **77** (1996) 4495–4498, [arXiv:hep-ph/9605332](#).
- [48] M. Hindmarsh, “Level set method for the evolution of defect and brane networks,” *Phys. Rev. D* **68** (2003) 043510, [arXiv:hep-ph/0207267](#).
- [49] T. Garagounis and M. Hindmarsh, “Scaling in numerical simulations of domain walls,” *Phys. Rev. D* **68** (2003) 103506, [arXiv:hep-ph/0212359](#).
- [50] E. W. Kolb and M. S. Turner, *The Early Universe*, vol. 69. Taylor and Francis, 5, 1990.
- [51] **Particle Data Group** Collaboration, S. Navas *et al.*, “Review of particle physics,” *Phys. Rev. D*

[110 \(2024\) 030001](#).

- [52] D. Baumann, *Cosmology*. Cambridge University Press, 7, 2022.
- [53] S. Blasi, A. Mariotti, A. Rase, A. Sevrin, and K. Turbang, “Friction on ALP domain walls and gravitational waves,” *JCAP* **04** (2023) 008, [arXiv:2210.14246 \[hep-ph\]](#).
- [54] S. Blasi, A. Mariotti, A. Rase, and A. Sevrin, “Axionic domain walls at Pulsar Timing Arrays: QCD bias and particle friction,” *JHEP* **11** (2023) 169, [arXiv:2306.17830 \[hep-ph\]](#).
- [55] L. Kawano, “Evolution of Domain Walls in the Early Universe,” *Phys. Rev. D* **41** (1990) 1013.
- [56] P. P. Avelino, C. J. A. P. Martins, and J. C. R. E. Oliveira, “One-scale model for domain wall network evolution,” *Phys. Rev. D* **72** (2005) 083506, [arXiv:hep-ph/0507272](#).
- [57] T. Hiramatsu, M. Kawasaki, K. Saikawa, and T. Sekiguchi, “Axion cosmology with long-lived domain walls,” *JCAP* **01** (2013) 001, [arXiv:1207.3166 \[hep-ph\]](#).
- [58] M. Maggiore, *Gravitational Waves. Vol. 1: Theory and Experiments*. Oxford University Press, 2007.
- [59] R. Z. Ferreira, A. Notari, O. Pujolas, and F. Rompineve, “Gravitational waves from domain walls in Pulsar Timing Array datasets,” *JCAP* **02** (2023) 001, [arXiv:2204.04228 \[astro-ph.CO\]](#).
- [60] C. Caprini *et al.*, “Detecting gravitational waves from cosmological phase transitions with LISA: an update,” *JCAP* **03** (2020) 024, [arXiv:1910.13125 \[astro-ph.CO\]](#).
- [61] C. Caprini, R. Durrer, T. Konstandin, and G. Servant, “General Properties of the Gravitational Wave Spectrum from Phase Transitions,” *Phys. Rev. D* **79** (2009) 083519, [arXiv:0901.1661 \[astro-ph.CO\]](#).
- [62] R. Z. Ferreira, S. Gasparotto, T. Hiramatsu, I. Obata, and O. Pujolas, “Axionic defects in the CMB: birefringence and gravitational waves,” *JCAP* **05** (2024) 066, [arXiv:2312.14104 \[hep-ph\]](#).
- [63] I. Dankovsky, E. Babichev, D. Gorbunov, S. Ramazanov, and A. Vikman, “Revisiting evolution of domain walls and their gravitational radiation with CosmoLattice,” *JCAP* **09** (2024) 047, [arXiv:2406.17053 \[astro-ph.CO\]](#).